

Phase Diagram of the Schwinger Model by Adiabatic Preparation of States on a Quantum Simulator

Oleg Kaikov ^{1,*} Theo Saporiti ¹ Vasily Sazonov ¹ and Mohamed Tamaazousti ¹

¹*Université Paris-Saclay, CEA, List, F-91120, Palaiseau, France*

(Dated: August 7, 2024)

We argue the feasibility to study the phase structure of a quantum physical system on quantum devices via adiabatic preparation of states. We introduce a novel method and successfully test it in application to the Schwinger model in the presence of a topological θ -term. We explore the first-order-phase-transition and the no-transition regions of the corresponding phase diagram. The core idea of the method is to separately evolve the ground and the first excited states with a time-dependent Hamiltonian, the time-dependence of which interpolates between different values of θ . Despite our approach being a direct application of the adiabatic theorem, in some cases we are able to demonstrate its advantages in comparison to a different method from the literature that also employs adiabatic state preparation.

I. INTRODUCTION

Within any physical theory, the phase diagram determines the behavior of the fields for any given parameter regime. The knowledge of the phase structure of a theory is therefore fundamental for the understanding of the physical phenomena that it models. Due to the complexity of many theories, their phase diagrams are often studied numerically. An approach commonly utilized for this task is that of Monte Carlo (MC) simulation. For example, this method has been successfully used to analyze certain parameter regimes within the phase diagram of lattice Quantum Chromodynamics (QCD) [1].

However, for lattice QCD (LQCD) this approach fails in the presence of a non-zero chemical potential [2, 3], resulting in a non-zero baryon density: The Boltzmann factor of the Euclidean path integral becomes complex. This factor can therefore no longer be reliably considered as a probability weight in MC algorithms. Such an occurrence of a negative or complex probability measure is referred to as the sign problem. In addition, a non-zero charge conjugation and parity symmetry (CP) violating topological θ -term in LQCD would also lead to the sign problem [4]. Thus, adhering to the MC method requires modifications [1]. However, other promising approaches [4–7], that are unaffected by the sign problem, are those of quantum computing and tensor networks. Considerable progress has already been achieved in this direction [8–17].

In this work we argue the feasibility to explore the phase diagram of the Schwinger model [18] with a non-zero topological θ -term by adiabatic preparation of states on a digitally simulated quantum device. Despite the fact that the Schwinger model is less expressive than QCD, the two models share many key properties. Therefore, on the one hand, the Schwinger model is easier to study. On the other hand, due to its similarity to QCD, the Schwinger model serves as a good benchmark theory for

testing various methods designed to be applied to QCD in the future.

Within the conventional lattice formulation, the presence of a topological θ -term in the Schwinger model renders the standard MC methods inapplicable due to the sign problem. Many analytic solutions have been developed in the literature. For example, there are methods based on a reformulation of the theory, allowing the use of the standard MC approach. These include, e.g., a dual formulation within the massless lattice Schwinger model with staggered fermions [19, 20], and the lattice formulation of the bosonized Schwinger model [21–23] for arbitrary fermion mass. In the present work, however, we explore the quantum computing approach.

In addition, the Schwinger model with a non-zero θ -term possesses a diverse phase structure including a first-order phase transition (PT) at $\theta = \pi$ for sufficiently large masses and a region without transitions in the sub-critical mass regime [24–33]. This makes the Schwinger model the perfect candidate to test our approach utilizing a quantum computer. Although analyses of the Schwinger model and its multi-flavor versions include different variational [33, 34] and adiabatic [30, 31, 35–38] methods, to the best of our knowledge, we are not aware of studies applying the method that we propose to this or any other model.

Variational approaches, such as the variational quantum eigensolver (VQE) [39], can be computationally cheaper in comparison to adiabatic methods. However, the choice of an appropriate variational ansatz often requires additional insight into the system being studied in order to exclude undesired sub-regions of the Hilbert space. Conversely, adiabatic methods can be comparatively simpler to employ, but, again, are often computationally more costly. Our method belongs to the latter category and is based on evolving multiple eigenstates with a time-dependent Hamiltonian, the time-dependence of which interpolates between different values of the considered parameter, which, in our case, is the value of θ .

In section II we briefly review the Schwinger model

* oleg.kaikov@cea.fr

in the continuum, its phase structure and its lattice discretization via staggered fermions. In section III we review the adiabatic theorem and expand on our method. In section IV we present the numerical results of our approach. In section V we discuss our method and compare it to a different method that utilizes adiabatic state preparation as well as a deformation of the Hamiltonian to avoid level crossings [40]. Last, in section VI we present our conclusions and an outlook on future work.

II. THE SCHWINGER MODEL

The Schwinger model is a (1+1)-dimensional $U(1)$ gauge theory. It describes quantum electrodynamics coupled to a single flavor of a massive Dirac fermion [18]. In this section we review the Hamiltonian formulation of the theory and the phase diagram of the model.

A. Continuum theory

We set $\hbar = c = 1$ throughout the work. The continuum Hamiltonian density of the Schwinger model in the presence of the θ -term reads

$$\mathcal{H} = -i\bar{\psi}\gamma^1(\partial_1 - igA_1)\psi + m\bar{\psi}\psi + \frac{1}{2}\left(\dot{A}_1 + \frac{g\theta}{2\pi}\right)^2. \quad (1)$$

Here, ψ is a two-component Dirac spinor. The components $\psi_\alpha(x)$, $\alpha = 1, 2$, obey the usual fermionic anti-commutation relations $\{\psi_\alpha^\dagger(x), \psi_\beta(y)\} = \delta(x-y)\delta_{\alpha\beta}$. The gauge field is denoted by A_μ , $\mu = 0, 1$, with the Hamiltonian density (1) written in the temporal gauge $A_0 = 0$. The parameters m and g denote the bare fermion mass and coupling, respectively. The two-dimensional γ^μ matrices obey the Clifford algebra $\{\gamma^\mu, \gamma^\nu\} = 2\eta^{\mu\nu}$, where $\eta = \text{diag}(1, -1)$. We adopt the convention $\gamma^0 = X$, $\gamma^1 = iZ$, with the standard Pauli matrices X and Z . We also identify $\bar{\psi} = \psi^\dagger\gamma^0$. The physical states of the theory satisfy Gauss's law

$$-\partial_1\dot{A}_1 = g\bar{\psi}\gamma^0\psi. \quad (2)$$

We now discuss the properties of the model. A non-zero θ -term in (1) results in a constant background electric field. The physics of the model is periodic in θ with a period of 2π . At $\theta = \pi$, there is a second-order PT at the critical mass in units of the coupling $m_c/g \approx 0.33$ and a first-order PT above m_c/g at the same value of θ [25–27, 41]. Qualitatively, this can be understood as follows: For $m/g \gg 1$ and a background electric field $\theta < \pi$, it is energetically costly to produce charged particles. Therefore, in this regime the ground state corresponds to a state with no particles. Contrarily, for $m/g \gg 1$ and a background electric field $\theta > \pi$ it is energetically favorable to produce a negatively charged particle on the left of the one-dimensional interval and a positively charged particle on the right. Correspondingly, the electric field

is reduced by one unit [25, 27]. These two parameter regions are separated by a first-order PT line at $\theta = \pi$ for $m/g \gg 1$, where the two corresponding ground states are degenerate in energy.

Conversely, for $m/g < m_c/g$ it is energetically more favorable to produce more pairs of charged particles. This screens the background electric field [42]. Therefore, there is no PT in this parameter region. The corresponding phase diagram of the Schwinger model is shown in Fig. 1(a).

B. Lattice formulation

To study the Schwinger model numerically we utilize the lattice discretization via Kogut-Susskind staggered fermions [43], following the recent work [33]. Here we closely recapitulate the main steps of [33]. In this formulation, the Schwinger model Hamiltonian on a lattice with an even number of sites N with spacing a and open boundary conditions (OBC) reads [43]

$$\begin{aligned} H = & -\frac{i}{2a} \sum_{n=0}^{N-2} (\phi_n^\dagger U_n \phi_{n+1} - \text{H.c.}) \\ & + m_{\text{lat}} \sum_{n=0}^{N-1} (-1)^n \phi_n^\dagger \phi_n \\ & + \frac{ag^2}{2} \sum_{n=0}^{N-2} (l_0 + L_n)^2. \end{aligned} \quad (3)$$

Here, ϕ_n is a single-component fermionic field obeying the anti-commutation relation $\{\phi_n^\dagger, \phi_{n'}\} = \delta_{nn'}$. The quantized dimensionless electric field operator L_n and the operator U_n act on the links that connect sites n and $(n+1)$. These two operators obey the commutation relation $[U_n, L_{n'}] = \delta_{nn'} U_n$. The parameters m_{lat} and g are the lattice mass and coupling, respectively. The background electric field is given by $l_0 = \theta/(2\pi)$.

On the lattice, the continuum Gauss's law (2) becomes

$$L_n - L_{n-1} = Q_n, \quad (4)$$

with the charge operator

$$Q_n = \phi_n^\dagger \phi_n - \frac{1}{2}(1 - (-1)^n). \quad (5)$$

Note that the total charge $\sum_{n=0}^{N-1} Q_n$ is conserved due to the global $U(1)$ symmetry of the theory.

Following [33], we set the electric field on the left boundary to zero. This can be done since a non-zero value can be viewed as a constant additive shift in the value of the background electric field. Using (4), the electric field on each link can then be expressed solely in terms of the fermionic charges as [33]

$$L_n = \sum_{k=0}^n Q_k. \quad (6)$$

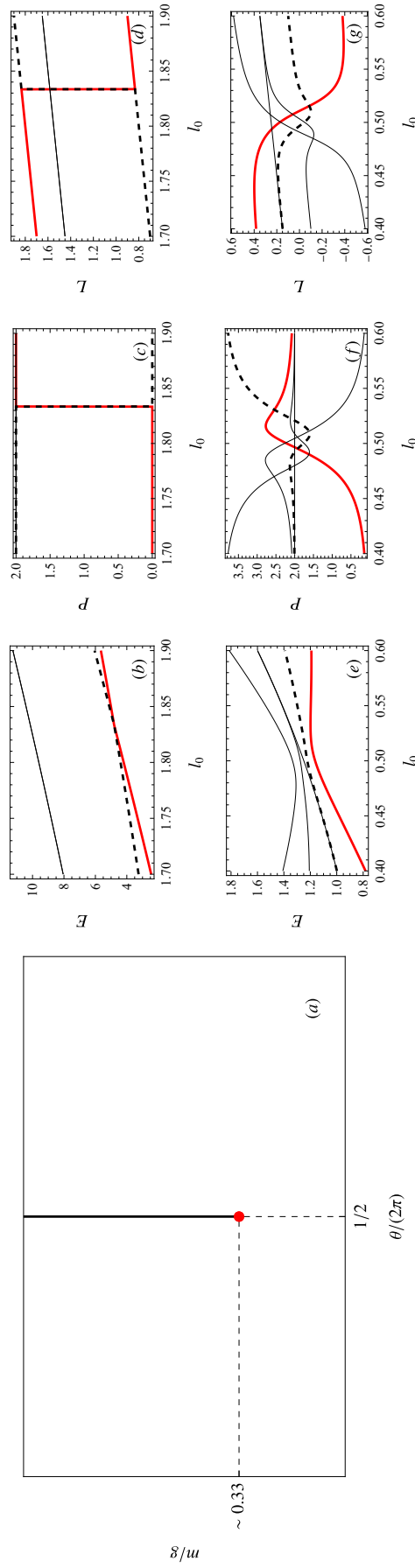


FIG. 1. Phase structure of the Schwinger model. Panel (a): phase diagram of the model in the θ - m/g plane. For $m/g > m_c/g \approx 0.33$ there is a first-order phase transition at $\theta = \pi$ (solid black line). This first-order phase transition line ends at m_c/g in a second-order phase transition (red point). Below m_c/g no transitions take place. Panels (b) - (g): exact diagonalization results (see section IV for numerical values of input parameters) for the eigenstate energy E (panels (b), (e)), particle number P (panels (c), (f)) and electric field density L (panels (d), (g)) for 10^3 steps over l_0 for a set of lowest eigenstates. The results for the ground state, first excited state and higher excited states are shown in solid red, dashed black and thin solid black, respectively. Panels (b) - (d): four lowest eigenstates for $m_{\text{lat}}/g = 10$ (above second-order phase transition). Panels (e) - (g): five lowest eigenstates for $m_{\text{lat}}/g = 0$ (below second-order phase transition).

We can therefore use this to eliminate the gauge fields and the corresponding operators U_n [44], such that the Hamiltonian in (3) becomes

$$H = -\frac{i}{2a} \sum_{n=0}^{N-2} (\phi_n^\dagger \phi_{n+1} - \text{H.c.}) + m_{\text{lat}} \sum_{n=0}^{N-1} (-1)^n \phi_n^\dagger \phi_n + \frac{ag^2}{2} \sum_{n=0}^{N-2} \left(l_0 + \sum_{k=0}^n Q_k \right)^2. \quad (7)$$

To translate the Hamiltonian (7) to qubits we apply the Jordan-Wigner transformation [45] with

$$\phi_n = \prod_{k < n} (iZ_k) \frac{1}{2} (X_n - iY_n), \quad (8)$$

where X_n , Y_n , Z_n are the usual Pauli operators acting on spin n . Applying the Jordan-Wigner transformation to the charge operator in (5) we obtain

$$Q_n = \frac{1}{2} (Z_n + (-1)^n). \quad (9)$$

We re-scale the Hamiltonian to make it dimensionless,

$$H \rightarrow \frac{2}{ag^2} H. \quad (10)$$

Last, to enforce the condition of vanishing total charge we add a penalty term to the Hamiltonian

$$H \rightarrow H + \lambda \left(\sum_{n=0}^{N-1} Q_n \right)^2, \quad (11)$$

while choosing the Lagrange multiplier λ sufficiently large.

The final lattice Hamiltonian is then given by [33]

$$H = \frac{x}{2} \sum_{n=0}^{N-2} (X_n X_{n+1} + Y_n Y_{n+1}) + \frac{1}{2} \sum_{n=0}^{N-2} \sum_{k=n+1}^{N-1} (N - k - 1 + \lambda) Z_n Z_k + \sum_{n=0}^{N-2} \left(\frac{N}{4} - \frac{1}{2} \left\lceil \frac{n}{2} \right\rceil + l_0 (N - n - 1) \right) Z_n + \frac{m_{\text{lat}}}{g} \sqrt{x} \sum_{n=0}^{N-1} (-1)^n Z_n + l_0^2 (N - 1) + \frac{1}{2} l_0 N + \frac{1}{8} N^2 + \frac{\lambda}{4} N, \quad (12)$$

where $x = 1/(ag)^2$ is the inverse lattice spacing squared in units of the coupling and $\lceil \cdot \rceil$ is the ceiling function.

The lattice discretization via staggered fermions requires an additive mass renormalization [46], such that the renormalized mass is given by

$$m_r/g = m_{\text{lat}}/g + \text{MS}(V, ag, l_0), \quad (13)$$

where MS is the additive mass shift and $V = N/\sqrt{x}$ is the dimensionless lattice volume.

For periodic boundary conditions (PBC) the mass shift was analytically computed in [46] to be

$$\text{MS}_p = \frac{1}{8\sqrt{x}}. \quad (14)$$

For OBC the mass shift is not analytically known. However, Ref. [32] introduced a method to compute it numerically. In addition, Ref. [32] argued that, for sufficiently large volumes V , (14) provides a good approximation also for OBC. As the mass shift does not play the central role in our analysis, we adopt the latter strategy and use (14) for the mass shift in (13) while setting $V = 30$ for the numerical simulations.

To detect a first-order PT or the absence thereof, we measure the energies of at least two of the lowest eigenstates over the l_0 region of interest and observe whether the corresponding levels cross or not when varying l_0 . For the completeness of our analysis, we also consider two additional observables [33]. One of these is the particle number operator

$$P = \frac{N}{2} + \frac{1}{2} \sum_{n=0}^{N-1} (-1)^n Z_n. \quad (15)$$

The other is the electric field density operator in the bulk

$$L = l_0 + \frac{1}{4} + \frac{1}{2} \sum_{n=0}^{N/2-2} Z_n + \frac{1}{4} Z_{N/2-1}. \quad (16)$$

In the latter, to reduce boundary effects, two neighboring links in the center of the system are considered. Furthermore, the discretization via staggered fermions causes a non-uniform electric flux on the links, due to the staggering of the charge on the lattice. Consequently, to reduce the boundary and the staggering effects, the electric field on two neighboring links in the center of the chain is averaged over [33].

The commutator of the particle number operator (15) and the Hamiltonian (12) vanishes only in the limit $m/g \gg 1$. Therefore, integer eigenvalues of P represent good quantum numbers only for large values of m/g [33, 47]. For $m/g \gg 1$ and $\theta < \pi$, the ground state is given by $|10\rangle^{\otimes N/2}$, with no particles present. Conversely, for $m/g \gg 1$ and $\theta > \pi$ the state containing a pair of particles, $|11\rangle \otimes |10\rangle^{\otimes (N-4)/2} \otimes |00\rangle$, corresponds to the ground state. Here, a negatively (positively) charged particle is localized on the left (right) of the one-dimensional chain at site 1 ($N - 2$). Panels (b) - (g) of Fig. 1 show energy E , particle number P and electric field density L over l_0 for a set of lowest eigenstates for m_{lat}/g above (panels (b) - (d)) and below (panels (e) - (g)) the second-order PT.

III. ADIABATIC PREPARATION OF STATES

A. Adiabatic theorem

Multiple versions of the adiabatic theorem exist in the literature. We choose to adopt a version motivated by some of the earliest formulations [48–56]. Specifically, consider a quantum system parameterized by a time-dependent Hamiltonian $H(t)$ and prepared in one of its instantaneous eigenstates. The adiabatic theorem states that the system remains in that state if: 1. The Hamiltonian is varied sufficiently slowly, and 2. There is a non-zero gap between the eigenvalue of that state and the rest of the spectrum for all t .

Many works have since expanded on the adiabatic theorem, see e.g. [57–60]. However, to keep our arguments general, we focus on the version stated above. Below we expand upon and quantify the conditions 1. and 2. to three different degrees of detail.

1. First formulation

At the most fundamental level, there are two characteristic time-scales at play. The first is the typical time-scale T_{dyn} of the system's intrinsic dynamics determined by the Hamiltonian. The second is the time-scale T on which the Hamiltonian itself is changed externally. Now, the time-scale of the dynamics within the system is governed by and is inversely proportional to the difference in the relevant energy levels. For the remainder of the paper, we define Δ to be the minimal energy gap between two of the relevant levels.

Using this, we can define a non-adiabaticity parameter,

$$\varepsilon \sim \frac{T_{\text{dyn}}}{T} \sim \frac{1}{\Delta T}, \quad (17)$$

which measures how non-adiabatic the evolution of the state is under a time-dependent Hamiltonian. For the evolution to be adiabatic, $\varepsilon \ll 1$ needs to hold. In other words, the variation in the Hamiltonian is then sufficiently slow, allowing the state to adjust to the changed system. For a given minimal energy gap Δ , we can equivalently express this as a condition on the time-scale T on which the Hamiltonian is to be evolved, $T \gg 1/\Delta$.

2. Second formulation

Having considered the condition of adiabaticity from the perspective of time-scales, we can also study it from the viewpoint of energies. Namely, for the evolution of the state to be adiabatic, the change in the system's energy over the typical time-scale of the intrinsic dynamics T_{dyn} needs to be much smaller than the minimal energy gap between the relevant levels. That is,

$$T_{\text{dyn}} |\langle \dot{H} \rangle| \ll \Delta, \quad (18)$$

where $\langle \dot{H} \rangle = \langle \psi(t) | \dot{H} | \psi(t) \rangle$ and $|\psi(t)\rangle$ is the time-evolved state. Note that this version of the adiabaticity condition is more expressive than (17), as it includes the information on how the energy of the system in a specific state changes when the Hamiltonian is varied.

Employing the fact that $T_{\text{dyn}} \sim 1/\Delta$ and approximating $|\langle \dot{H} \rangle| \sim \Delta/T$, from (18) we can estimate $T \sim \Delta/|\langle \dot{H} \rangle| \gg 1/\Delta$, recovering the result of the first formulation. That is, we can now express the non-adiabaticity parameter at a higher degree of accuracy as

$$\varepsilon \sim \frac{|\langle \dot{H} \rangle|}{\Delta^2}. \quad (19)$$

This is the estimate that we utilize in our numerical analysis in section IV.

3. Third formulation

For completeness, we also review a further formulation, variations of which are common in the literature [61–64]. We again denote the Hamiltonian of a quantum system as $H(t)$ and its state as $|\psi(t)\rangle$. We consider the system's evolution according to the Schrödinger equation on a finite time-interval, with $t \in [0, T]$. Here, a parameter of the Hamiltonian is externally varied in time. For example, in the Schwinger model lattice Hamiltonian (12), the parameter that is varied in time is the background electric field, such that $l_0 = l_0(t)$.

Now, let $|E_\alpha; t\rangle$ be the instantaneous eigenstates of $H(t)$ with corresponding eigenvalues $E_\alpha(t)$, satisfying

$$H(t) |E_\alpha; t\rangle = E_\alpha(t) |E_\alpha; t\rangle. \quad (20)$$

Here, α labels the different eigenstates, with $\alpha = 0$ corresponding to the ground state. Consider, for simplicity, that we prepare the system at $t = 0$ in the ground state $|E_0; 0\rangle$. Furthermore, assume that there is a non-zero gap between $E_0(t)$ and the rest of the spectrum for all values of t . Then the probability to find the system not in the ground state at time $t \in [0, T]$, i.e. the transition probability, is

$$p_{\text{tr}}(t) = 1 - |\langle E_0; t | \psi(t) \rangle|^2. \quad (21)$$

An estimate of an upper bound on $p_{\text{tr}}(t)$ is commonly given by [61, 62]

$$p_{\text{tr}}(t) \lesssim \max_{t \in [0, T]} \frac{|\langle E_1; t | \frac{dH}{dt} | E_0; t \rangle|}{(E_1(t) - E_0(t))^2}. \quad (22)$$

To make a connection to the second formulation in (19), we can estimate

$$p_{\text{tr}}(t) \lesssim \frac{|\langle \dot{H} \rangle|}{\Delta^2} \sim \varepsilon. \quad (23)$$

That is, in this formulation, from $\varepsilon \ll 1$ we indeed recover the simplified adiabaticity condition $T \gg 1/\Delta$ as well as a suppressed transition probability $p_{\text{tr}}(t) \ll 1$.

B. Evolving through a phase transition

In the previous section we considered the case of a non-zero gap between the eigenvalue of the evolved state and the rest of the spectrum for all values of t . However, what would the time-evolution of the state correspond to, when the gap is zero for some value of t ? For example, in the specific case of a level crossing. This question is motivated by the large- m_{lat}/g regime of the Schwinger model (see Fig. 1(b)).

Below we first consider the regime of large but finite m_{lat}/g , supported by the numerical results shown in Fig. 1(b). Here we also quantitatively define the question we would like to answer. Second, we consider the strict limit $m_{\text{lat}}/g \gg 1$, without corrections from the kinetic term of the Hamiltonian. Third, we highlight the similarities and the differences of the large but finite m_{lat}/g regime and the $m_{\text{lat}}/g \gg 1$ limit. Last, we summarize and discuss our findings.

1. The large- m_{lat}/g regime

Consider first the large- m_{lat}/g regime of the lattice Schwinger model in (12). As Fig. 1(b) shows, the two lowest levels cross, causing a first-order PT in the system. Clearly, the condition of a non-zero gap is not satisfied in this case and, according to its definition in section III A, the adiabatic theorem is not applicable.

From Fig. 1(b) we furthermore observe that the second and higher excited states have much higher energies than those of the two lowest levels for the entire considered range of l_0 . Therefore, during the time-evolution of each of the two lowest states with a time-dependent Hamiltonian the probability to transition into the higher states is negligible. We can thus restrict our analysis to that of the two lowest levels only.

The question we would like to answer is the following: Take the ground state at l_0^{\min} as the initial state at $t = 0$. Then evolve this state over $t \in [0, T]$ according to the Schrödinger equation

$$i \frac{d}{dt} |\psi(t)\rangle = H(t) |\psi(t)\rangle, \quad (24)$$

with the Hamiltonian (12) and a linear ramp given by

$$l_0(t) = l_0^{\min} + \frac{l_0^{\max} - l_0^{\min}}{T} t. \quad (25)$$

The question is now, what is the evolved state $|\psi(T)\rangle$? That is, do we stay on the same level throughout the time-evolution, or is there a non-zero probability to transition to the new ground state? Furthermore, does this probability depend on T ?

2. The limit $m_{\text{lat}}/g \gg 1$

We answer the above question in the context of a specific example: We consider a simplified abstract scenario of a system of two levels, corresponding to the limit $m_{\text{lat}}/g \gg 1$.

This is supported by the observation from our numerical results for large m_{lat}/g that, for all values of l_0 within the relevant range, the two eigenstates with the lowest energies are well approximated by the two states of section II B; $|10\rangle^{\otimes N/2}$ and $|11\rangle \otimes |10\rangle^{\otimes (N-4)/2} \otimes |00\rangle$.

Let us emphasize the difference between the large m_{lat}/g and $m_{\text{lat}}/g \gg 1$: The large- m_{lat}/g regime involves finite values of this parameter, whereas in the strict limit $m_{\text{lat}}/g \gg 1$ there are no corrections from the kinetic term of the Hamiltonian.

Let us justify restricting the problem to two levels more thoroughly. In the limit $m_{\text{lat}}/g \gg 1$ the kinetic term of the Hamiltonian can be neglected, and therefore the particle number operator P in (15) commutes with the Hamiltonian (12). That is, for large m_{lat}/g the Hamiltonian is predominantly diagonal in the eigenbasis of P . The integer eigenvalues of P are thus good quantum numbers in the large- m_{lat}/g regime. In the vicinity of the PT, the two lowest levels correspond to 0 and 2 particles. In the case where there are 2 particles, these are localized on sites 1 and $(N-2)$. It is therefore meaningful to write the Hamiltonian of our two-level problem in the basis of $\{|01\rangle, |10\rangle\}$ for sites 1 and $(N-2)$. As the particle number operator commutes with the Hamiltonian on the entire considered domain of l_0 in the $m_{\text{lat}}/g \gg 1$ limit, the corresponding Hamiltonian for the problem is diagonal in this basis for all l_0 .

We therefore consider the Hamiltonian given by

$$\tilde{H}(l_0) = \begin{pmatrix} E_i(l_0) & 0 \\ 0 & E_{ii}(l_0) \end{pmatrix}, \quad (26)$$

constructed in the basis of $\{|01\rangle, |10\rangle\}$. Here, “i” and “ii” denote the two levels, where $\tilde{H}(l_0) |01\rangle = E_i(l_0) |01\rangle$ and $\tilde{H}(l_0) |10\rangle = E_{ii}(l_0) |10\rangle$. In the specific case that the levels cross and do so only once at a critical value $l_0^* \in [l_0^{\min}, l_0^{\max}]$, we have $E_i(l_0^{\min}) < E_{ii}(l_0^{\min})$, $E_i(l_0^{\max}) > E_{ii}(l_0^{\max})$ and $E_i(l_0) = E_{ii}(l_0) \Leftrightarrow l_0 = l_0^*$ ¹.

Clearly, evolving the ground state $|01\rangle$ at l_0^{\min} according to the Schrödinger equation (24) with $l_0 = l_0(t)$ for $t \in [0, T]$ will result in the same state for any value of T , up to a global phase. Evidently, an analogous statement

¹ More generally, the two-level Hamiltonian in (26) is in fact even more expressive. The continuous functions $E_i(l_0)$ and $E_{ii}(l_0)$ can depend arbitrarily on l_0 . Therefore, this Hamiltonian can describe, for example, a system where the levels cross, or where they have a single common point without crossing, or where there is a non-zero energy gap between the levels. The specific dependence of $E_i(l_0)$ and $E_{ii}(l_0)$ on l_0 correspondingly determines how $|\psi(t)\rangle$ evolves.

holds for the state $|10\rangle$. That is, we will remain on the same level that we started with. Indeed,

$$\begin{aligned} |\psi(T)\rangle &= e^{-i \int_0^T E_i(t) dt} |01\rangle, \\ |\psi(T)\rangle &= e^{-i \int_0^T E_{ii}(t) dt} |10\rangle \end{aligned} \quad (27)$$

are both solutions of (24). Note that for any value of T , that is, irrespective of how slowly the Hamiltonian is varied, we remain in the initial state (up to a global phase). Therefore, for this particular two-level problem, evolving both of the levels separately with a time-dependent Hamiltonian, we can recover the phase-transition point by identifying it with the point where the two levels cross.

3. Back to the finite- m_{lat}/g regime

Now, let us come back to the lattice Schwinger model for large but finite m_{lat}/g . Here, although the two lowest-energy eigenstates can be well approximated by $|10\rangle^{\otimes N/2}$ and $|11\rangle \otimes |10\rangle^{\otimes (N-4)/2} \otimes |00\rangle$, the former are not identically equal to the latter. Furthermore, clearly, the rest of the system beyond the two lowest levels and the interactions within it cannot in general be completely ignored for any finite value of m_{lat}/g .

In other words, the above two-level problem is a highly simplified example. Nevertheless, it provides us with the valuable information that in some particular cases, such as the $m_{\text{lat}}/g \gg 1$ limit of the lattice Schwinger model, it may be possible to recover the first-order PT point by evolving multiple states with a time-dependent Hamiltonian.

4. Discussion and summary

Let us remark that within the larger class of Hamiltonians that possess level crossings, which can be more general than in the example above (e.g. include interactions), there exists a certain sub-set of systems with the following property: When an eigenstate is evolved on a finite time-scale T with a time-dependent Hamiltonian, the probability to transition into a different level is bounded from above by $\mathcal{O}(T^{-\gamma})$ for an appropriate $\gamma \geq 0$ [49, 57]. Therefore for such systems we are also able to detect the first-order PT by individually evolving the levels.

We now come back to the specific example considered before. Let us reiterate the purpose of this two-level problem. We do not claim that all two-level systems that possess a level crossing correspond to the Hamiltonian (26). Rather, we provide a constructive existence proof that there exist systems that possess a level crossing and allow to find a PT point by evolving multiple

levels. For further examples see the overview of [57] and references therein.

In summary, consider a scenario where we possess no knowledge about the phase structure of the system (see section V for a more detailed discussion). Assume that evolving multiple levels of this system for some finite time T we observe a level crossing. One alternative is that the evolution has not been sufficiently adiabatic, and the system transitioned from one state to another upon passing over a relatively small non-zero gap. That is, here we are not sufficiently sensitive to resolve the small gap. However, the other alternative is that we may have indeed recovered a true level crossing. The possibility of the latter is demonstrated by the above simplified two-level example and supported by the examples presented in [57] and references therein.

In general, the system is, of course, likely to have a more intricate level structure, with many excited states in the proximity of the ground state, multiple crossings of various levels, requiring to evolve more than two levels with a very gradual variation of the parameter, in order to recover the phase structure of the model. More generally, we may also only be given a Hamiltonian without any additional information. That is, ultimately, we may not a priori know if the levels cross, have a single common point without crossing or whether there is a non-zero gap. Still, let us emphasize that finding a first-order PT is one of the possible outcomes of the application of this procedure. Below we expand on the method in more detail.

C. Adiabatic evolution of multiple states

Here we present our method, as well as a specific version of it implemented in Algorithm 1. We first introduce the algorithm and subsequently expand on the general approach. Throughout Algorithm 1, when it is executed on a quantum device or simulator, we assume that the time-step size, the Suzuki-Trotter order of the decomposition as well as the number of shots are chosen such that the evolution depends sufficiently weakly on the variation of these parameters (see discussion below).

The input of the algorithm consists of: First, the parameter range $[p_{\min}, p_{\max}]$ that is to be studied. Second, the time-dependent Hamiltonian of the system $H(p(t))$, which includes the dependence of the parameter p on time, according to the chosen ramp. The ramp sweeps over the parameter range, such that $p(t=0) = p_{\min}$ and $p(t=T) = p_{\max}$. Third, a set of lowest-energy eigenstates $\{|S\rangle\}$ at the boundary of the parameter range p_{\min} . Fourth, an initial value for the total evolution time T_{in} . Fifth, a strictly monotonically increasing function $f: T \rightarrow T' > T$, which determines how the total evolution time is increased for each iteration of the algorithm. Sixth, a user-defined bound \mathcal{B} on the average Euclidean point-wise distance over p of the same energy level between two consecutive iterations of the algorithm,

summed over all considered energy levels.

We define this normalized average norm between two computations of the same energy levels $l_s(p)$, corresponding to two consecutive iterations of the algorithm, as

$$\mathcal{E} = \frac{1}{\epsilon \mathcal{N}} \sum_s \|l_s^{\text{old}}(p) - l_s(p)\|. \quad (28)$$

Here s labels the level corresponding to the state $|s\rangle \in \{|S\rangle\}$. The Euclidean norm is given by

$$\|l_s^{\text{old}}(p) - l_s(p)\| = \sqrt{\sum_{i=1}^{\mathcal{N}} (l_s^{\text{old}}(p_i) - l_s(p_i))^2}. \quad (29)$$

To calculate this norm, the result $l_s(p)$ of the new iteration is interpolated over p , and evaluated over the set of \mathcal{N} parameter points of the old result $l_s^{\text{old}}(p)$. Note that \mathcal{N} depends on the iteration of the algorithm with

$$\mathcal{N} = \dim(\{p\}) \text{ of } l_s^{\text{old}}(p). \quad (30)$$

In (28) we normalize with respect to the difference

$$\epsilon = \frac{1}{\mathcal{N}} \sum_s \|l_s^{\text{1st}}(p) - l_s^{\text{2nd}}(p)\| \quad (31)$$

of the respective levels between the first and the second iterations of the algorithm. Here $\mathcal{N} = \dim(\{p\})$ of $l_s^{\text{1st}}(p)$.

The algorithm terminates when the Euclidean norm becomes smaller than the user-set total error bound, $\mathcal{E} < \mathcal{B}$. Note that this does not guarantee that the levels converge to their true dependence on p . Instead, this means that the dependence of the levels on p is not affected by the current value of T sufficiently enough for $\mathcal{E} \geq \mathcal{B}$ to hold.

Within the algorithm, in order to compute the value and the position of the minimal energy gap, we define the level $l_g(p)$ as that corresponding to the ground state at p_{\min} . Finally, the output of the algorithm is as follows: First, the final total evolution time T , for which $\mathcal{E} < \mathcal{B}$ is satisfied. Second, the value of the minimal energy gap Δ . Third, the corresponding parameter value p_Δ . That is, p_Δ is such that the gap has a value of Δ at p_Δ .

It is advantageous to adapt the algorithm to the specific problem at hand. In case we possess no knowledge about the system, except for the Hamiltonian itself and the spectrum at p_{\min} , we cannot, in general, guarantee the convergence of our algorithm towards the true phase structure of the model. If we are provided with more information, we may be able to introduce a criterion to guarantee convergence. The specifics are case-dependent.

For example, in the best-case scenario when we know the underlying phase structure (e.g. by exact diagonalization) and would like to verify it, instead of using (28) we can calculate the Euclidean norm with respect to the exact diagonalization (ED) results for each individual iteration,

$$\tilde{\mathcal{E}} = \frac{1}{\tilde{\epsilon} \mathcal{N}} \sum_s \|l_s^{\text{ED}}(p) - l_s(p)\|. \quad (32)$$

Algorithm 1: Evolution of multiple states

Input: Parameter range $[p_{\min}, p_{\max}] \ni p$, Hamiltonian $H(p(t))$, set of lowest-energy eigenstates $\{|S\rangle\}$ at p_{\min} , initial value for total evolution time T_{in} , strictly monotonically increasing function $f: T \rightarrow T' > T$, error bound \mathcal{B}

Output: Final evolution time T , minimal gap Δ and corresponding parameter value p_Δ

```

T ← Tin;
ε ← B;
while ε ≥ B do
  for |s⟩ ∈ {|S⟩} do
    evolve |s⟩ with H(p(t)) for t ∈ [0, T];
    ls(p) ← ⟨s(t)| H(p(t)) |s(t)⟩;
  end
  if T > Tin then
    if T = f(Tin) then
      ε ← 1/ℳ ∑s ||lsold(p) - ls(p)||;
    end
    ε ← 1/(εℳ) ∑s ||lsold(p) - ls(p)||;
  end
  T ← f(T);
  lsold(p) ← ls(p);
  ℳ ← dim({p}) of lsold(p);
end
g ← s' such that ls'(pmin) = min|s⟩ ∈ {|S⟩} [ls(pmin)];
if lg(p) crosses with any other ls(p) for s ≠ g then
  Δ ← 0;
  find pΔ by interpolating corresponding levels;
else
  Δ ← minp ∈ [pmin, pmax], |s⟩ ∈ {|S⟩}, |s⟩ ≠ |g⟩ [ls(p) - lg(p)];
  pΔ ← arg minp ∈ [pmin, pmax], |s⟩ ∈ {|S⟩}, |s⟩ ≠ |g⟩ [ls(p) - lg(p)];
end

```

Here, ϵ from (31) is accordingly modified to

$$\tilde{\epsilon} = \frac{1}{\mathcal{N}} \sum_s \|l_s^{\text{ED}}(p) - l_s^{\text{1st}}(p)\|, \quad (33)$$

and \mathcal{N} is now given by $\mathcal{N} = \dim(\{p\})$ of $l_s(p)$, with the Euclidean norm evaluated over the set of points of $l_s(p)$, correspondingly.

At its core, our method is a direct application of the adiabatic theorem. Let us assume the following base scenario: We are given a Hamiltonian and the parameter range of the “interesting” regime, where one of the following occurs for the two lowest levels: A single level crossing, a single common point of the levels without a level crossing, or a minimal non-zero gap. However, we are not given the information about which of the above it is and for which value of the parameter it occurs. In addition, all higher levels possess much higher energies than the lowest two on the entire parameter range. We proceed as follows: We find the two lowest eigenstates

on one boundary of the parameter range and evolve the states separately with a time-dependent Hamiltonian for a (relatively short) chosen time T , sweeping over the parameter range.

Here we may or may not observe a level crossing. If we detect a non-zero gap or a single common point after which the levels again diverge, then we have found a strong indication that the two levels in the corresponding parameter regime do not cross. If, however, we observe a level crossing, there are two options: First, we may have indeed recovered a true level crossing and a corresponding first-order PT. Second, however, it is also possible that the evolution time T has not been sufficiently long, i.e. the evolution has not been slow enough to be adiabatic. In this latter case, for example, the state may have transitioned from the ground state into a higher excited state, upon passing over a comparatively small non-zero energy gap.

We therefore increase the evolution time T and repeat the procedure. We continue iterating the scheme over greater values of T until we either: 1. Observe a non-zero gap or a single point of contact and are thus able to guarantee convergence, or, 2. Exhaust our computational resources.

Outcome 1: If we converge to a result of a non-zero gap or a single point of contact between the two levels, we have successfully achieved our goal of discovering a region of the phase diagram and observed that no first-order PT takes place in that regime. Outcome 2: If, however, we have exhausted the computational capabilities and still observe a level crossing, we again cannot conclude with certainty whether we have found a true level crossing or the evolution has not been slow enough.

Let us note that the opposite cannot occur. That is, having observed a non-zero gap for a certain value of T , we cannot observe a level crossing for a greater value of T . This is because finding a gap informs us that the current value of T has been sufficiently large for the evolution to be sensitive enough to resolve this gap. Increasing T would only improve this sensitivity, again leading to the observation of a finite gap.

We can track the differences in the levels from iteration to iteration for increasing values of T by means of (28). If we observe that these consecutive differences diminish, this implies that from iteration to iteration the parameter-dependence of the levels is less and less affected by the total evolution time T , or, equivalently, by the measure ε of the non-adiabaticity of the process. It is nevertheless important to emphasize that although a convergence of the levels towards an independence on T may take place, this does not necessarily imply a convergence to the underlying true parameter-dependence of the levels.

However, the process of iterating the procedure for increasing values of T is one of the advantages of this method. Specifically, while this is a necessary requirement for testing the reliability of any method that utilizes adiabatic state preparation without any prior knowl-

edge of the true parameter-dependence of the state, the present method incorporates this as part of the investigative procedure itself. We expand on this in more detail in section V A and compare our method with a different method from the literature.

In addition, when the procedure is being carried out on a quantum device, for each value of T one should vary the time-step size δt (optionally, the Suzuki-Trotter order of the decomposition as well), and the number of shots n_{shots} , until the change due to this variation is sufficiently small. Note that, again, without prior knowledge of the time-evolution, this too is a necessary measure for any adiabatic state preparation algorithm on a quantum computer.

In case we are not given any information except for the Hamiltonian, we may need to evolve more than two levels very slowly and over large parameter ranges. However, on the contrary, if we are provided with additional information, our method correspondingly gains more predictive power. We discuss this in more detail in section V.

Nevertheless, if we find a point on the phase diagram for which there is a minimal non-zero energy gap between the levels, we can use this to our advantage. Namely, using (19), we are then able to provide an estimate of the upper bound on the gap in the vicinity of the corresponding point on the phase diagram (see section IV B for specific example).

To optimize our method, it is possible to modify the linear ramp of (25) and instead consider a local ramp, such as that in [40], with an additional lower bound on the ramp speed for the case of level crossings. To implement a greater part of the method on a quantum device, the initial states for the adiabatic evolution can be prepared using the variational quantum deflation (VQD) [65] or subspace search VQE (SSVQE) [66] methods. This is especially advantageous in a scenario when it is comparatively easy to construct the low-energy eigenstates in a well-understood regime and then to evolve these states into the less well-understood parameter sub-region.

IV. NUMERICAL ANALYSIS

For the numerical analysis of the Schwinger model lattice Hamiltonian in (12) we perform three types of simulations: First, ED using QuSpin [67–69]. Second, adiabatic state preparation using QuTiP [70–72], which we call “time-evolution on a classical device”. Third, adiabatic state preparation using Qiskit [73] on a classical computer which we call “time-evolution on a digital quantum simulator”.

The input parameters of the model common for all three types of simulations are the following: The total site number is $N = 6$, the dimensionless lattice volume is $V = 30$ and the Lagrange multiplier is $\lambda = 100$. We found this value of λ to be sufficient to ensure a vanishing total charge in our simulations. The ED simulations in Figs. 1, 2 and 3 are performed with 10^3 steps. For

the adiabatic state preparation simulations via (24) we employ the linear ramp from (25). For the strictly monotonically increasing function $f: T \rightarrow T' > T$ we choose the following sequence: For the first nine iterations i of the algorithm we take

$$T_i = 5i, \quad 1 \leq i \leq 9. \quad (34)$$

For the subsequent iterations we use the recursion relation

$$T_i = 10T_{i-9}, \quad i \geq 10. \quad (35)$$

The time-step size is constant throughout and is given by $\delta t = 0.5$. This results in the number of time-steps given by $n_{\delta t, i} = 2T_i$ for each corresponding simulation. Consequently, l_0 is varied more slowly for a greater value of T . The corresponding $l_{0,i}$ -step size for an algorithm iteration i is given by $\delta l_{0,i} = (l_0^{\max} - l_0^{\min})/n_{\delta t, i}$.

The time-evolution on a digital quantum simulator is subject to shot-induced noise, with $n_{\text{shots}} = 10^4$ shots per circuit. Furthermore, for the quantum simulator we set the order of the Suzuki-Trotter decomposition [74, 75] equal to $q_{\text{ST}} = 6$ throughout.

Note that the time-step size δt , the l_0 -step size δl_0 , the number of steps $n = n_{\delta t} = n_{\delta l_0}$, the total evolution time $T = n\delta t$ and the Suzuki-Trotter order q_{ST} are all co-dependent parameters. That is, to make the parameter sweep more adiabatic by increasing T while keeping δt fixed, we need to increase n . Although this reduces δl_0 for a fixed range $[l_0^{\min}, l_0^{\max}]$, this also increases the error of the Trotter expansion (TE) after time T , with the corresponding error given by $\epsilon_{\text{TE}} = T(\delta t)^{q_{\text{ST}}}$. To prevent this error from increasing, while maintaining the new value for T with a fixed δt , the Suzuki-Trotter order q_{ST} needs to be increased.

Last, for the quantum simulator the initial states at l_0^{\min} are prepared by ED. To implement a greater part of the simulation on a quantum device, the states from the spectrum used as initial states can instead be obtained using VQD [65] or SSVQE [66].

For completeness, in addition to the eigenstate energy E , we also compute the particle number P from (15) and the electric field density L from (16) for all three types of simulations. Below we present the results of our numerical analysis.

A. Regime above the second-order phase transition

The numerical results for $m_{\text{lat}}/g = 10$ for the sub-set of the total evolution times $T \in \{5, 50, 500\}$ are shown in Fig. 2. We observe that the two lowest levels cross (see section IV C for the continuation of this discussion). Correspondingly, we indeed recover the first-order PT. This agrees with the ED results. Furthermore, note from the ED results shown in Fig. 1(b) that the higher excited states have a much higher energy, making the probability to transition into them negligible. This is verified by the

results shown in the first and second columns of Fig. 2. The former shows the probability $p_{0,\alpha} = |\langle E_\alpha; t | \psi(t) \rangle|^2$ to find the ground state $|E_0; 0\rangle$ at l_0^{\min} evolved under (24) in the instantaneous eigenstate $|E_\alpha; t\rangle$ of $H(t)$ at a time t . The latter similarly shows $p_{1,\alpha} = |\langle E_\alpha; t | \psi(t) \rangle|^2$ for the evolved first excited state $|E_1; 0\rangle$ at l_0^{\min} .

We are therefore able to successfully validate the method described in section III C in a particular setting. Namely, our method recovered the previously known result of a level crossing and a corresponding first-order PT on the given range of l_0 . Moreover, we were able to recover the corresponding critical value l_0^* where the first-order PT takes place. Below we first discuss the results of our numerical analysis in the no-transition region of the phase diagram. We then consider the dependence of the errors \mathcal{E} and $\tilde{\mathcal{E}}$ on the iteration of the algorithm for both regimes.

B. Regime below the second-order phase transition

The results for the regime $m_{\text{lat}}/g = 0$ are presented in Fig. 3. We observe that as T is increased, the dependence of the two lowest levels on l_0 obtained by our method approaches the ED results. Specifically, we successfully recover the non-zero gap between the two lowest levels. Here, the slow convergence of the adiabatic results towards those of ED is due to the size of the gap as well as the proximity in energy of the higher excited states to the two lowest levels (see Fig. 1(e)).

In this example, again, using our adiabatic method, we successfully recover the known dependence of the energy levels on l_0 . Namely, we verify that indeed there are no PTs on this range of l_0 . Moreover, we are able to find the minimal value of the non-zero energy gap between the ground state and the rest of the spectrum on this l_0 -range.

Since we are able to recover the occurrence of an energy gap, this implies that at the end of the algorithm the evolution of state has been sufficiently adiabatic. This allows us to calculate from (19) the value of ε which is sufficient for adiabaticity. That is, we can compute ε for certain parameter regions where we have found a non-zero energy gap, and use it for neighboring parameter regions as an estimate of the expected relation between T and Δ . The value of ε obtained in this way provides a lower bound on the energy gap that we are able to resolve by evolving the system over a time T . That is, ε is a measure of non-adiabaticity, and it decreases with increasing T . If we are able to find a non-zero gap for some minimal value of T , this provides us with an estimate for the measure of the maximal non-adiabaticity $\varepsilon_{\text{suff}}$ that is still sufficient for the evolution process to be adiabatic.

Specifically, based on the above result, we can perform several estimates that inform us of the system's behavior for similar values of m_{lat}/g and l_0 . We can use this to our advantage when scanning neighboring sub-regions of the phase diagram. In particular, from (19) we can estimate

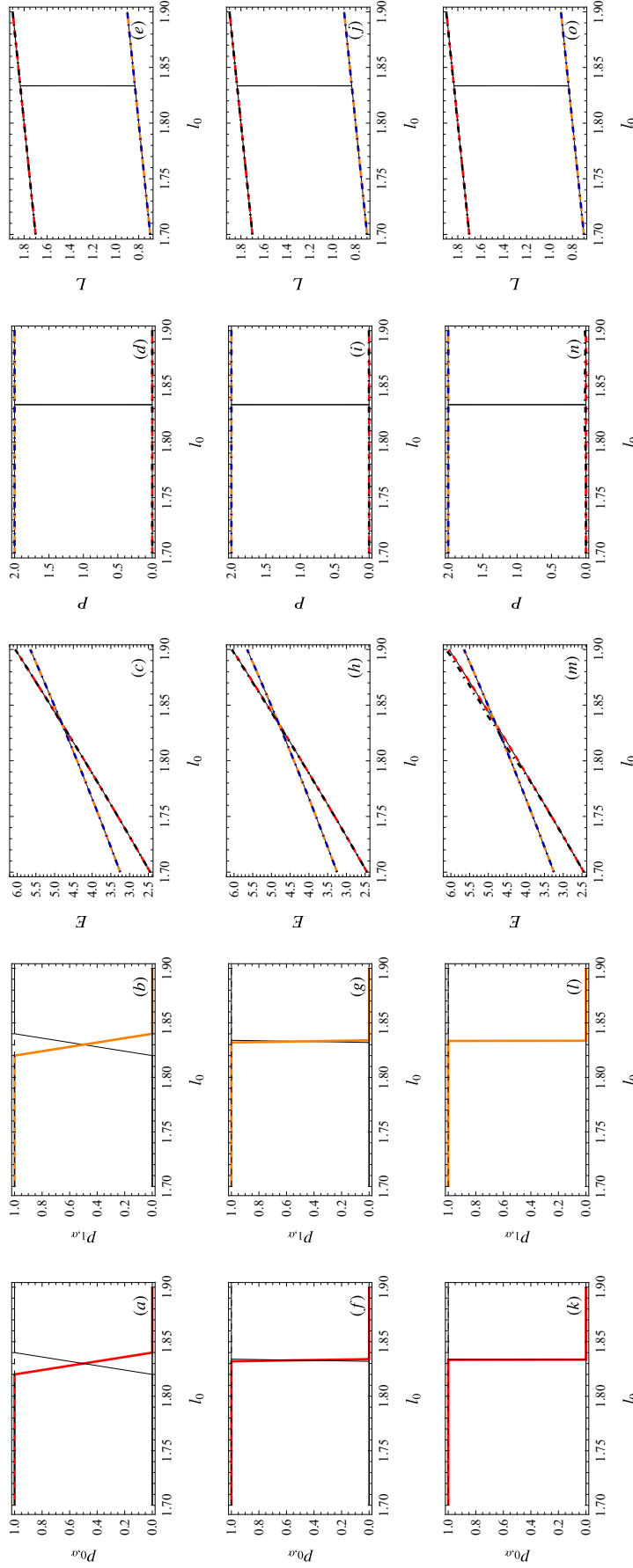


FIG. 2. First-order phase transition in the regime above the second-order phase transition. Here we set $m_{\text{lat}}/g = 10$. Top, middle and bottom rows show the results for $T = 5, 50$ and 500 , respectively. The first column (from the left) shows the time-evolution of the ground state at $l_0^{\text{min}} = 1.7$ evolved according to (24) with (12) and (25) from $l_0^{\text{min}} = 1.7$ to $l_0^{\text{max}} = 1.9$ on a classical device. The respective panels show the probability $p_{0,\alpha}$, plotted over l_0 , to find the evolved state in the various instantaneous eigenstates $|E_\alpha; t\rangle$ at a corresponding l_0 . The probability to remain in the ground state is shown in solid black. The probabilities to transition to each of the three lowest excited states depicted in Figs. 1(b) - 1(d) are shown in thin solid black. The total probability of the above four lowest eigenstates is shown in thin dashed black. The second column shows the analogous probability $p_{1,\alpha}$ for the evolved first excited state at $l_0^{\text{min}} = 1.7$. The probability to remain in the first excited state is shown in solid orange. Third, fourth and fifth columns show the eigenstate energy E , particle number P and electric field density L over l_0 , respectively. The results of exact diagonalization for the two lowest states are shown in thin solid black. The results for the evolution of the two lowest states at $l_0^{\text{min}} = 1.7$ on a classical device (digital quantum simulator) are shown in dashed red and dashed orange (dash-dotted black and dash-dotted blue), respectively.

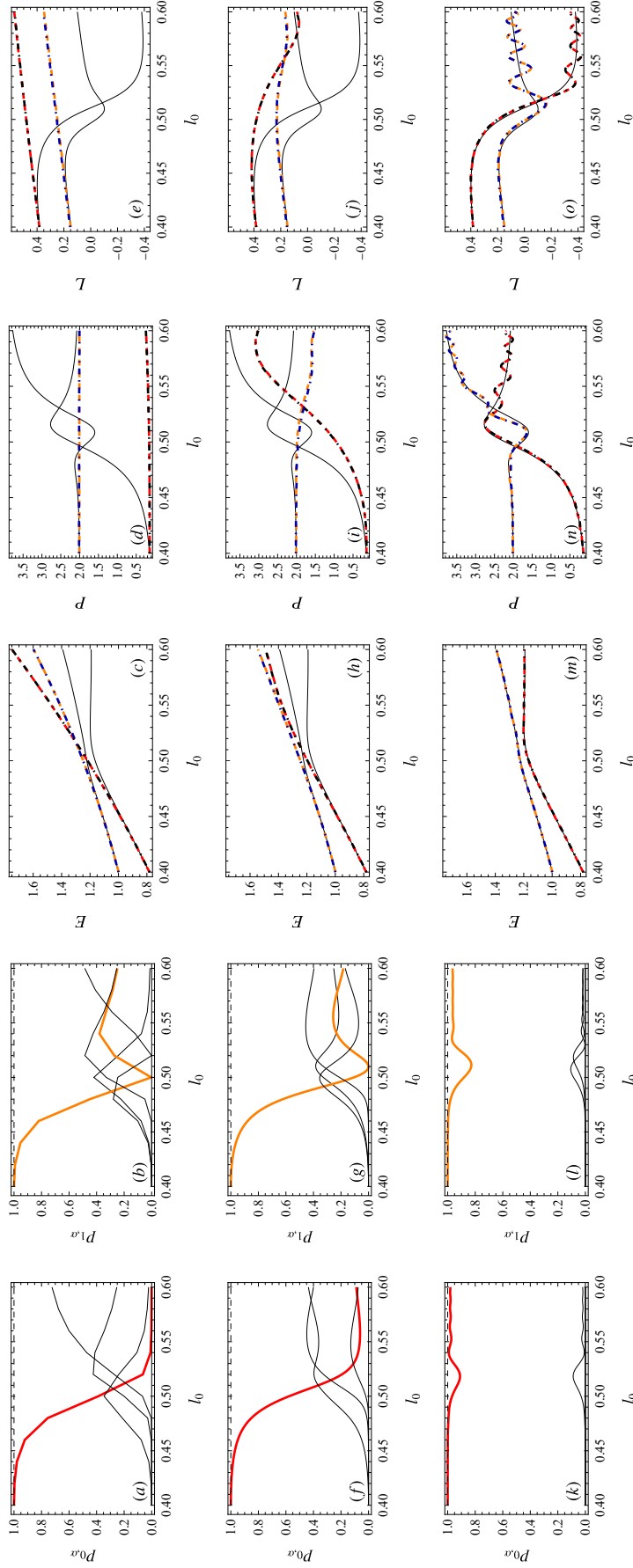


FIG. 3. No phase transition in the regime below the second-order phase transition. Here we set $m_{\text{lat}}/g = 0$. For the panels in the first and second columns we consider the five lowest eigenstates depicted in Figs. 1(e) - 1(g). We evolve the two lowest eigenstates at $l_0^{\text{min}} = 0.4$ according to (24) with (12) and (25) from $l_0^{\text{min}} = 0.4$ to $l_0^{\text{max}} = 0.6$. In all other aspects the description follows that of Fig. 2.

the upper bound on the value of ε that is still sufficient for adiabaticity as

$$\varepsilon_{\text{suff}} \approx \frac{1}{T} \frac{E_{\text{diff}}}{\Delta^2}. \quad (36)$$

Here, we estimate $|\langle \dot{H} \rangle| \approx E_{\text{diff}}/T$, where E_{diff} is the difference in energies of the evolved states between the beginning and the end of the time-evolution.

From our numerical results we obtain the following specific values on the corresponding l_0 range:

$$\begin{aligned} T &= 5 \times 10^2, \\ E_{\text{diff}} &\approx E_1(l_0^{\text{max}}) - E_0(l_0^{\text{min}}) \approx 6.10 \times 10^{-1}, \\ \Delta &\approx 4.80 \times 10^{-2}. \end{aligned} \quad (37)$$

With these numerical values we obtain from (36)

$$\varepsilon_{\text{suff}} \approx 5.30 \times 10^{-1}. \quad (38)$$

Note that $\varepsilon \ll 1$ is still consistent with our estimate of $\varepsilon_{\text{suff}}$, since the latter is an upper bound on the non-adiabaticity parameter ε . In fact, the obtained result signifies that the obtained value of $\varepsilon_{\text{suff}}$ is still sufficient for adiabaticity.

We can use (38) to reformulate (36) as an estimate of the lower bound on the expected evolution time T for a given gap as

$$T \gtrsim \frac{1}{\varepsilon_{\text{suff}}} \frac{E_{\text{diff}}}{\Delta^2} \sim \frac{1.15}{\Delta^2}. \quad (39)$$

Equivalently, given a chosen evolution time T , we can estimate the lower bound on the gap that we are able to resolve,

$$\Delta \gtrsim \sqrt{\frac{1.15}{T}}. \quad (40)$$

We have thus obtained an estimate of the gap that we are able to resolve (or, equivalently, of the minimal required evolution time) for near-lying values of m_{lat}/g and l_0 . Of course, this estimate will vary depending on the specific values of the parameters.

The fact that the time-evolution has been sufficiently adiabatic is also supported by the values we obtain for the probabilities to remain in the corresponding initial states; $p_{0,\alpha=0}(T) \approx 0.98$ and $p_{1,\alpha=1}(T) \approx 0.96$ from Figs. 3(k) and 3(l), respectively.

Although not perfectly consistent with adiabaticity, the minimal probabilities (on the entire l_0 range) to remain in the initial states $p_{0,\alpha=0}^{\text{min}} \approx 0.91$ and $p_{1,\alpha=1}^{\text{min}} \approx 0.83$ are nevertheless sufficiently large to ensure that for each individual simulation, at the end of the time-evolution at $t = T$, the system is found in a state that lies in the proximity of the level corresponding to the initial state. This is because the energy gap increases again as l_0 approaches $l_0(T) = l_0^{\text{max}}$. In addition, the oscillations of P and L in Figs. 3(n) and 3(o), respectively, result from an imperfect overlap of the desired ideal target eigenstate obtained from ED and the actual evolved state (cf. Figs. 3(k) and 3(l)).

C. Convergence analysis

In this section we consider the deviation \mathcal{E} in (28) between two consecutive iterations of the algorithm, as well as the deviation $\tilde{\mathcal{E}}$ in (32) of each individual iteration of the algorithm from the corresponding ED result. The results are shown in Fig. 4. Here, since we are able to analyze the system by ED, we are able to evaluate with certainty how our adiabatic method performs by comparing it with the true dependence of the energy levels on l_0 .

Based on the results shown in Fig. 4, let us remark that an increase of the deviation \mathcal{E} between consecutive iterations (orange and blue lines) does not determine whether $\tilde{\mathcal{E}}$ (red and black lines) increases or decreases. Instead, a greater value of \mathcal{E} simply means that the absolute difference between consecutive iterations increased.

From the results in Fig. 4(a) for $m_{\text{lat}}/g = 0$, we observe that both the evolution on a classical device as well as that on a digital quantum simulator approach the ED results as T is increased (red and black lines, respectively). Furthermore, we observe that for T approaching 500 the difference between consecutive iterations both on a classical device and on a digital quantum simulator decreases. That is, the dependence of the levels on l_0 becomes less affected by the value of T . This further supports the validity of our results.

However, the results in Fig. 4(b) for $m_{\text{lat}}/g = 10$ differ considerably. First, the deviation of the evolution on a classical device from the ED results (red line) does not decrease to zero for T approaching 500. This occurs because the levels cross and, correspondingly, the gap between them is zero for some value of l_0 . Due to this, there is mixing that takes place between the levels, irrespective of how large the value of T is.

Second, the deviation of the evolution on a digital quantum simulator from the ED results (black line) increases. Moreover, clearly, the results obtained on the digital quantum simulator (black line) differ from those obtained on a classical device (red line). Consistently, the corresponding differences between two consecutive iterations on a classical device and on a digital quantum simulator (orange and blue lines, respectively) differ as well.

The reason for this mismatch lies in the difference of the methods employed in simulations performed on the classical device and on the digital quantum simulator. On the classical device, the solution for the time-evolution of a state is obtained by the integration of the set of ordinary differential equations determined by the system. On the digital quantum simulator the approach is different: This method utilizes Trotter expansion and is additionally affected by shot-induced noise. The fact that we observe the above discrepancies for the case of a level crossing and not in the case of a non-zero gap, suggests that these are gap-dependent.

To test whether this effect occurs because of the size of the Trotter step as well as due to the shot-induced

noise, we perform supplementary simulations, where we vary the input parameters. The results are shown in Figs. 4(c), 4(d), 4(e), 4(f). Panel (c) shows the results of panel (b) on the domain $T \in [5, 50]$, this is the baseline for the comparison.

From panel (c) to panel (d) the change is that we decrease the Trotter step from 0.5 to 0.05. We observe that the digital quantum simulator (black line) now performs better for larger T , as $\tilde{\mathcal{E}}$ decreases. However, the result still differs from that of the classical device (red line). From panel (c) to panel (e) we remove the shot-induced noise from the simulation. Here, in fact, the digital quantum simulator performs worse for all T . Last, in panel (f) we decrease the time-step to 0.05 and remove the shot-induced noise as well. Here we observe that the results of the classical device and of the digital quantum simulator match. This indicates that decreasing the size of the Trotter step as well as increasing the number of shots should improve the results on the digital quantum simulator. That is, we find evidence that our method can be successfully applied both on classical and on quantum devices.

V. DISCUSSION

A. Comparison with the deformation method

In this section we briefly review the adiabatic method of [40] and specify its similarities and differences to our method.

To find where the level crossing occurs, the idea of the method in [40], which we refer to as the “deformation method”, is the following: First, introduce into the Hamiltonian an additional term with a corresponding external parameter, such that the level crossings are avoided. Second, perform multiple simulations for decreasing values of the external parameter, determining the critical value of the other parameter originally responsible for the first-order PT (i.e. the analog of I_0^* for the Schwinger model). In [40], for the considered example of the XY model, this corresponds to the midpoint of the step in the magnetization, which plays the role of the order parameter. Third, to find the first-order PT point, extrapolate the obtained results into the limit of vanishing external parameter.

Before we highlight the differences of the two approaches, let us first comment on common properties of the methods. The two approaches share a common advantage: Since both algorithms employ adiabatic preparation of states, it is reasonable to apply them to a problem where the spectrum can be easily found in a certain well-studied region of the parameter space, and more difficult to find in a less-investigated region that we would want to explore.

For a further common property, recall the discussion of section III C: In order to ensure that an algorithm utilizing adiabatic state preparation on a quantum de-

vice performs correctly, we need to find indications for the convergence of the time-evolution when varying the number of shots n_{shots} , the time-step δt and the total evolution time T . If the true phase structure is known, the convergence concerns recovering the ED results. If the phase structure is unknown, the convergence refers to the dependence of the energy levels on the parameter the variation of which is responsible for the PT. Let us again emphasize that the manifestation of the latter does not imply that the former holds. However, note that while in each of the above cases the respective requirement is a necessary condition for the deformation method, it is also a sufficient condition for the application of our method. That is, the requirement of reliability of the method, which is tested by increasing T , is part of the procedure itself. We now consider a further distinction of the two approaches.

A particular distinction between the two methods becomes evident when the corresponding algorithms are executed on a quantum device. The deformation method requires adding an extra term to the Hamiltonian. First, clearly, this requires an understanding of what term to add. In general, this requires some analytic effort and knowledge of the system. Second, more importantly, adding any non-zero term to the Hamiltonian necessitates including additional corresponding gates into the circuit. On near-term quantum hardware this entails amplifying the sources of errors occurring on the quantum device.

Conversely, however, for a system with many level crossings, such as that studied in [40], our method would require evolving a number of states much larger than only two, if the parameter range to be explored is broad. Below we expand on further differences of the two methods in detail, with the numerical results of section IV at hand.

In particular, it is instructive to compare our method with the adiabatic method of [40] based on the information that we are provided with for a given problem and the task at hand. The differences of the two methods are best characterized when categorized according to the amount and type of information that we a priori possess about the problem.

Here we identify three classes (or levels), depending on our knowledge of the system. To be specific, in each class we make the distinction between the two cases when the true behavior of the system is given by a first-order PT and when there is a non-zero energy gap. For simplicity, we consider the case of a system of only two energy levels.

In general, if we know that there is a first-order PT in the region of interest, we would like to find the parameter value for which it occurs. If we know that there is a non-zero gap, we would like to verify this and find its specific value. Finally, if we have no knowledge of the system, we would like to learn anything about its phase structure that we can.

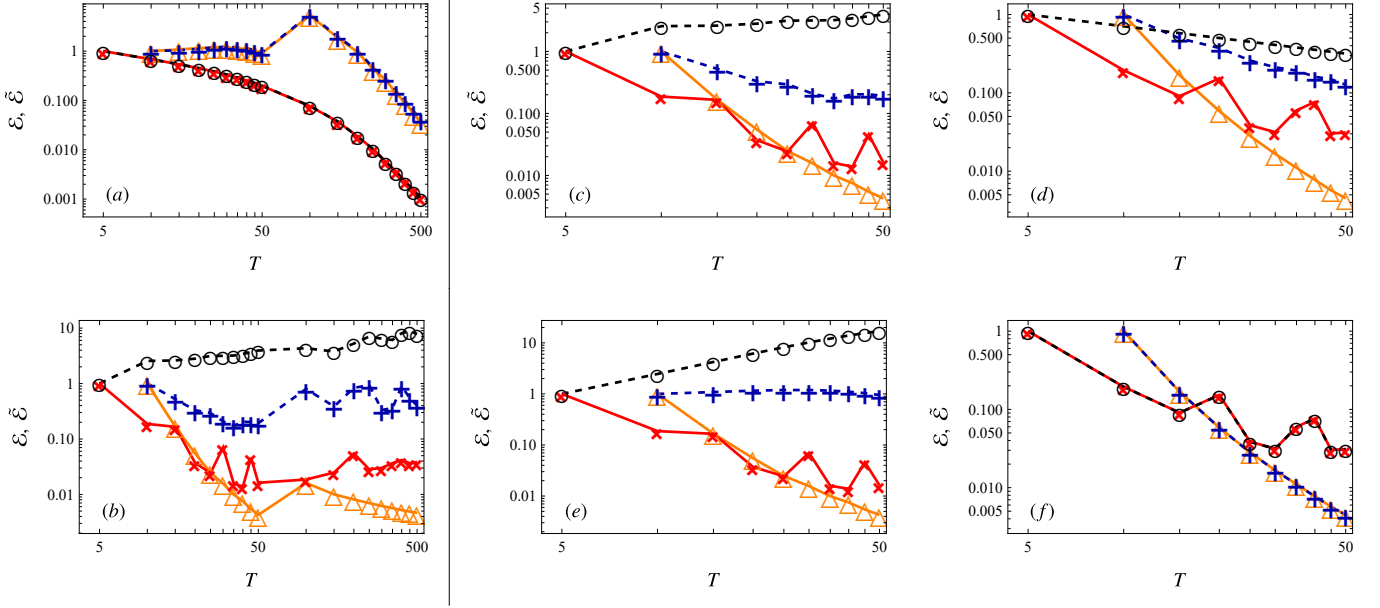


FIG. 4. Errors \mathcal{E} and $\tilde{\mathcal{E}}$ over evolution time T . The errors \mathcal{E} , calculated from (28), between two consecutive iterations on a classical device and on a digital quantum simulator are shown as orange \triangle -s and blue $+$ -s, respectively. The errors $\tilde{\mathcal{E}}$ calculated from (32) between the evolution on a classical device (digital quantum simulator) and exact diagonalization results are shown in red \times -s (black \circ -s). Panel (a) shows the results for $m_{\text{lat}}/g = 0$ for the parameter values set at the beginning of section IV. Panel (b): same as panel (a), but for $m_{\text{lat}}/g = 10$. On the right side of the divider, panels (c), (d), (e) and (f) show the results for $m_{\text{lat}}/g = 10$ with the following changes of parameter values: Panel (c): time-step $\delta t = 0.5$, $n_{\text{shots}} = 10^4$ shots for shot-induced noise (same as in panel (b)). Panel (d): $\delta t = 0.05$, $n_{\text{shots}} = 10^4$. Panel (e): $\delta t = 0.5$, without shot-induced noise. Panel (f): $\delta t = 0.05$, without shot-induced noise.

B. Dependence of the method on the knowledge about the system

1. Level 1: Perfect knowledge of the system

At the “easiest” level, we possess perfect knowledge of the system, i.e. we know the phase structure for the parameter range that is of interest to us. Here, we would like to verify our understanding using the two adiabatic methods. In the case where we know that there is a minimal non-zero gap and we know its position and value, there is no need to deform the Hamiltonian. Therefore, both methods amount to performing the adiabatic state preparation for the two levels separately. Moreover, using (19), we can provide an estimate for the lower bound on T .

Now consider the case where we know that the gap is zero and that there is a crossing at a known value of the parameter. To recover the known results, following the deformation method, we add an auxiliary term to the Hamiltonian and, after confirming the reliability of the method by varying T such that it is sufficiently large, execute the algorithm for the ground state at least two times in order to perform the extrapolation. Applying our method, however, after T is confirmed to be sufficiently large, we run the corresponding algorithm exactly

two times - once for each of the two lowest levels.

2. Level 2: Limited knowledge of the system

At this intermediate level, we have some knowledge of the phase diagram, for example from analytic considerations. Specifically, if we know that there is a non-zero gap, but we do not know its value and/or for which parameter value it is minimal, again, there is no need to deform the Hamiltonian and the strategy here is similar to that of *Level 1* above.

Furthermore, if we find a non-zero gap for a specific parameter choice, we can use this to our advantage: For a given T , the expression in (19) provides us with an estimate on the upper bound on the energy gap. We can use this to estimate the T - Δ dependence for neighboring regions in the parameter space of the model.

If there is a level crossing at an unknown value of the parameter, the procedures for the two adiabatic methods are the same as for *Level 1*.

3. Level 3: No knowledge of the system

For this level, which is the most challenging, we assume that we have no knowledge of the phase structure of the system. Specifically, consider the case when we don't know whether there is a first-order PT or a minimal non-zero gap for some value of the parameter. Moreover, we have no knowledge of the corresponding critical parameter value.

Regarding the deformation method we note the following: If we deform the Hamiltonian and apply the corresponding algorithm, we may erroneously conclude that there is a first-order PT where, in fact, there is none. Therefore, the deformation method is not applicable in this case.

However, this is where the procedure defined in [IIIC](#) gains a clear advantage. Indeed, the application of this method remains viable for the present scenario: We evolve the two lowest levels and, if we observe a non-zero gap, we can argue to have found the underlying phase structure of the model for a specific parameter choice. Conversely, if we have exhausted our computational resources and still observe a level crossing, this indicates that there *may* be a first-order PT, but this cannot be concluded with certainty. Furthermore, if we discover a neighboring parameter region with a non-zero gap, from [\(19\)](#) we can provide an estimate of the upper bound on the gap for the new parameter region being investigated.

Although the scenario of no knowledge of the system is hypothetically possible, as discussed previously, analytical arguments, such as whether one expects a first-order transition to occur or not, can greatly improve the predictive power of the methods. In the case that we truly know nothing about the system except for the Hamiltonian and the spectrum at one end of the parameter range, if we observe a level crossing, we cannot guarantee that this is indeed a true first-order PT. However, a physical model is usually constructed with some physical phenomenon or a defining characteristic in mind. This information may allow us to improve the interpretation of the results we obtain numerically.

C. Limitations of the method

Here we briefly recapitulate the limitations of our method. First, while our method can be advantageous if the two lowest energy levels are separated from the rest of the spectrum by a large gap, more computational resources will be required if the higher excited levels lie close to, or cross with, the lower two. In this case more states need to be evolved. If the underlying phase structure is a priori known to exhibit many level crossings involving multiple levels, such that each level can be identified with the ground state only for a short parameter range, the method of [\[40\]](#) may be more suitable for the task.

Second, if the phase structure is unknown, with our

method, the result of finding the true phase structure for a chosen set of model parameters can only be guaranteed if we observe a non-zero gap. If the levels cross, the result is inconclusive at worst. However, in this case, at best, we can provide an upper bound on the energy gap that we are unable to resolve, if we have discovered a non-zero gap for a neighboring parameter region.

Third, the procedure is likely to be computationally costlier than the variational methods, such as VQE. However, if little is known about the ground state in the “interesting” parameter regime, and the variational ansatz circuit therefore cannot be restricted to a sub-region of the Hilbert space that is polynomial in the number of qubits, our method may be a viable option.

VI. CONCLUSIONS AND OUTLOOK

In this work we introduced a new method for studying the phase structure of a quantum physical system on a quantum device. In particular, we applied it to investigate two distinct regimes: First, the occurrence of a first-order phase transition when varying a corresponding parameter of the model. Second, the absence of any transition where the ground state is separated from the rest of the spectrum by a non-zero energy gap.

The method is based on a direct application of the adiabatic theorem: We evolve individually the states from a sub-set of the lowest levels of the model with a time-dependent Hamiltonian, sweeping over the parameter range. If we are a priori given sufficient information about the system at hand, we are able to recover and verify the existing results, i.e. to confirm either the occurrence of a level crossing and a corresponding first-order phase transition, or a minimal non-zero energy gap.

If we have no knowledge of the phase structure of the system, we achieve one of the following two outcomes: In the best-case scenario, we find a non-zero energy gap between the levels and can thus conclude to have discovered the phase structure for a given parameter choice of the model. In the worst-case scenario, we have exhausted our computational capabilities while still observing a level crossing. Here, if we have previously found a non-zero gap for a neighboring choice of model parameters, using [\(19\)](#) we are able to provide an estimate of the upper bound on the energy gap for the new region of parameter space.

We have successfully tested this method in application to the Schwinger model in the presence of a topological θ -term. In this parameter regime, conventional Monte Carlo algorithms can no longer be applied reliably due to the manifestation of the sign problem. Specifically, we considered two parameter regions. First, high lattice mass-to-coupling ratio m_{lat}/g with a corresponding first-order phase transition. Second, low m_{lat}/g , below the critical value, for which no transitions occur.

We compared this method with a different known method [\[40\]](#) from the literature that also utilizes adia-

batic state preparation. We have highlighted the similarities of the two methods and discussed their differences. In particular, our method gains an advantage when executed on current and near-term quantum devices. Specifically, in comparison to [40], our method does not require introducing additional terms into the Hamiltonian and, consequently, additional gates into the circuit that may lead to an increase in errors on quantum hardware.

In terms of future work, there are several promising directions. One of these is to consider various error mitigation schemes, such as, for example, zero-noise extrapolation [76–79] and global randomized error cancellation [80] in application to the existing variational approaches [33]

and our adiabatic method, and to compare them.

ACKNOWLEDGMENTS

This work has received support from the French State managed by the National Research Agency under the France 2030 program with reference ANR-22-PNCQ-0002. We acknowledge the use of IBM Quantum services for this work. The views expressed are those of the authors, and do not reflect the official policy or position of IBM or the IBM Quantum team. O.K. would like to thank Stefan Kühn, Takis Angelides and Pranay Naredi for discussions on the Schwinger model and its implementation.

-
- [1] O. Philipsen, *Status of lattice studies of the QCD phase diagram*, *Prog. Theor. Phys. Suppl.* **174**, 206 (2008).
 - [2] P. de Forcrand, *Simulating QCD at finite density*, *PoS LAT2009*, 010 (2010).
 - [3] K. Nagata, *Finite-density lattice QCD and sign problem: Current status and open problems*, *Prog. Part. Nucl. Phys.* **127**, 103991 (2022).
 - [4] M. C. Bañuls and K. Cichy, *Review on novel methods for lattice gauge theories*, *Rep. Prog. Phys.* **83**, 024401 (2020).
 - [5] M. C. Bañuls, R. Blatt, J. Catani et al., *Simulating lattice gauge theories within quantum technologies*, *Eur. Phys. J. D* **74**, 165 (2020).
 - [6] L. Funcke, T. Hartung, K. Jansen, and S. Kühn, *Review on quantum computing for lattice field theory*, *PoS LATTICE2022*, 228 (2023).
 - [7] J. C. Halimeh, M. Aidelsburger, F. Grusdt et al., *Cold-atom quantum simulators of gauge theories*, *arXiv:2310.12201* (2023).
 - [8] E. A. Martinez, C. A. Muschik, P. Schindler et al., *Real-time dynamics of lattice gauge theories with a few-qubit quantum computer*, *Nature* **534**, 516 (2016).
 - [9] B. Yang, H. Sun, R. Ott et al., *Observation of gauge invariance in a 71-site Bose–Hubbard quantum simulator*, *Nature* **587**, 392 (2020).
 - [10] D. Paulson, L. Dellantonio, J. F. Haase et al., *Simulating 2D effects in lattice gauge theories on a quantum computer*, *PRX Quantum* **2**, 030334 (2021).
 - [11] L. B. Otfelie, M. Urbanek, M. Metcalf et al., *Simulating quantum materials with digital quantum computers*, *Quantum Sci. Technol.* **6**, 043002 (2021).
 - [12] S. Thompson and G. Siopsis, *Quantum computation of phase transition in the massive Schwinger model*, *Quantum Sci. Technol.* **7**, 035001 (2022).
 - [13] N. H. Nguyen, M. C. Tran, Y. Zhu et al., *Digital quantum simulation of the Schwinger model and symmetry protection with trapped ions*, *PRX Quantum* **3**, 020324 (2022).
 - [14] W.-Y. Zhang, Y. Liu, Y. Cheng et al., *Observation of microscopic confinement dynamics by a tunable topological θ -angle*, *arXiv:2306.11794* (2023).
 - [15] A. Di Meglio, K. Jansen, I. Tavernelli et al., *Quantum computing for high-energy physics: State of the art and challenges. Summary of the QC4HEP working group*, *arXiv:2307.03236* (2023).
 - [16] R. C. Farrell, M. Illa, A. N. Ciavarella, and M. J. Savage, *Quantum simulations of hadron dynamics in the Schwinger model using 112 qubits*, *arXiv:2401.08044* (2024).
 - [17] R. C. Farrell, M. Illa, A. N. Ciavarella, and M. J. Savage, *Scalable circuits for preparing ground states on digital quantum computers: The Schwinger model vacuum on 100 qubits*, *PRX Quantum* **5**, 020315 (2024).
 - [18] J. Schwinger, *Gauge invariance and mass. II*, *Phys. Rev.* **128**, 2425 (1962).
 - [19] C. Gattringer, T. Kloiber, and V. Sazonov, *Solving the sign problems of the massless lattice Schwinger model with a dual formulation*, *Nucl. Phys. B* **897**, 732 (2015).
 - [20] D. Göschl, C. Gattringer, A. Lehmann, and C. Weis, *Simulation strategies for the massless lattice Schwinger model in the dual formulation*, *Nucl. Phys. B* **924**, 63 (2017).
 - [21] I. Bender, H. J. Rothe, and K. D. Rothe, *Monte Carlo study of screening versus confinement in the massless and massive Schwinger model*, *Nucl. Phys. B* **251**, 745 (1985).
 - [22] H. Ohata, *Monte Carlo study of Schwinger model without the sign problem*, *J. High Energ. Phys.* **2023**, 7 (2023).
 - [23] H. Ohata, *Phase diagram near the quantum critical point in Schwinger model at $\theta = \pi$: Analogy with quantum Ising chain*, *Prog. Theor. Exp. Phys.* **2024**, 013B02 (2023).
 - [24] S. Coleman, R. Jackiw, and L. Susskind, *Charge shielding and quark confinement in the massive Schwinger model*, *Ann. Phys.* **93**, 267 (1975).
 - [25] S. Coleman, *More about the massive Schwinger model*, *Ann. Phys.* **101**, 239 (1976).
 - [26] C. Hamer, J. Kogut, D. Crewther, and M. Mazzolini, *The massive Schwinger model on a lattice: Background field, chiral symmetry and the string tension*, *Nucl. Phys. B* **208**, 413 (1982).
 - [27] T. M. R. Byrnes, P. Sriganesh, R. J. Bursill, and C. J. Hamer, *Density matrix renormalization group approach to the massive Schwinger model*, *Phys. Rev. D* **66**, 013002 (2002).
 - [28] V. Azcoiti, E. Follana, E. Royo-Amondarain et al., *Massive Schwinger model at finite θ* , *Phys. Rev. D* **97**, 014507 (2018).

- (2018).
- [29] L. Funcke, K. Jansen, and S. Kühn, *Topological vacuum structure of the Schwinger model with matrix product states*, *Phys. Rev. D* **101**, 054507 (2020).
 - [30] M. Honda, E. Itou, Y. Kikuchi et al., *Classically emulated digital quantum simulation for screening and confinement in the Schwinger model with a topological term*, *Phys. Rev. D* **105**, 014504 (2022).
 - [31] G. Pederiva, A. Bazavov, B. Henke et al., *Quantum state preparation for the Schwinger model*, *PoS LAT-TICE2021*, 047 (2022).
 - [32] T. Angelides, L. Funcke, K. Jansen, and S. Kühn, *Computing the mass shift of Wilson and staggered fermions in the lattice Schwinger model with matrix product states*, *Phys. Rev. D* **108**, 014516 (2023).
 - [33] T. Angelides, P. Naredi, A. Crippa et al., *First-order phase transition of the Schwinger model with a quantum computer*, *arXiv:2312.12831* (2024).
 - [34] M. C. Bañuls, K. Cichy, J. I. Cirac et al., *Density induced phase transitions in the Schwinger model: A study with matrix product states*, *Phys. Rev. Lett.* **118**, 071601 (2017).
 - [35] S. Kühn, J. I. Cirac, and M. C. Bañuls, *Quantum simulation of the Schwinger model: A study of feasibility*, *Phys. Rev. A* **90**, 042305 (2014).
 - [36] A. Yamamoto, *Toward dense QCD in quantum computers*, *PoS LATTICE2021*, 122 (2022).
 - [37] B. Chakraborty, M. Honda, T. Izubuchi et al., *Classically emulated digital quantum simulation of the Schwinger model with a topological term via adiabatic state preparation*, *Phys. Rev. D* **105**, 094503 (2022).
 - [38] D. Ghim, M. Honda, *Digital quantum simulation for spectroscopy of Schwinger model*, *arXiv:2404.14788* (2024).
 - [39] A. Peruzzo, J. McClean, P. Shadbolt et al., *A variational eigenvalue solver on a photonic quantum processor*, *Nat. Commun.* **5**, 4213 (2014).
 - [40] A. Francis, E. Zelleke, Z. Zhang et al., *Determining ground-state phase diagrams on quantum computers via a generalized application of adiabatic state preparation*, *Symmetry* **14**(4), 809 (2022).
 - [41] B. Buyens, S. Montangero, J. Haegeman et al., *Finite-representation approximation of lattice gauge theories at the continuum limit with tensor networks*, *Phys. Rev. D* **95**, 094509 (2017).
 - [42] C. Adam, *Massive Schwinger model within mass perturbation theory*, *Ann. Phys.* **259**, 1 (1997).
 - [43] J. Kogut and L. Susskind, *Hamiltonian formulation of Wilson's lattice gauge theories*, *Phys. Rev. D* **11**, 395 (1975).
 - [44] C. J. Hamer, Z. Weihong, and J. Oitmaa, *Series expansions for the massive Schwinger model in Hamiltonian lattice theory*, *Phys. Rev. D* **56**, 55 (1997).
 - [45] P. Jordan and E. P. Wigner, *Über das Paulische Äquivalenzverbot*, *Z. Phys.* **47**, 631 (1928).
 - [46] R. Dempsey, I. R. Klebanov, S. S. Pufu, and B. Zan, *Discrete chiral symmetry and mass shift in the lattice Hamiltonian approach to the Schwinger model*, *Phys. Rev. Res.* **4**, 043133 (2022).
 - [47] B. Buyens, J. Haegeman, F. Hebenstreit et al., *Real-time simulation of the Schwinger effect with matrix product states*, *Phys. Rev. D* **96**, 114501 (2017).
 - [48] P. Ehrenfest, *Adiabatische Invarianten und Quantentheorie*, *Ann. Phys.* **356**, 327 (1916).
 - [49] M. Born and V. Fock, *Beweis des Adiabatenatzes*, *Z. Phys.* **51**, 165 (1928).
 - [50] L. D. Landau, *Zur Theorie der Energieübertragung. II*, *Z. Sowjetunion* **2**, 46 (1932).
 - [51] C. Zener, *Non-adiabatic crossing of energy levels*, *Proc. R. Soc. Lond. A* **137**, 696 (1932).
 - [52] E. C. G. Stueckelberg, *Theorie der unelastischen Stöße zwischen Atomen*, *Helvetica Physica Acta* **5**, 369 (1932).
 - [53] E. Majorana, *Atomi orientati in campo magnetico variabile*, *Nuovo. Cim.* **9**, 43 (1932).
 - [54] T. Kato, *On the adiabatic theorem of quantum mechanics*, *J. Phys. Soc. Jpn.* **5**, 435 (1950).
 - [55] A. Messiah, *Mécanique quantique*, Tome 2, (Dunod, 1964).
 - [56] D. J. Griffiths, *Introduction to quantum mechanics*, (Prentice Hall, 1995).
 - [57] J. E. Avron and A. Elgart, *Adiabatic theorem without a gap condition*, *Comm. Math. Phys.* **203**, 445 (1999).
 - [58] S. Teufel, *A note on the adiabatic theorem without gap condition*, *Lett. Math. Phys.* **58**, 261 (2001).
 - [59] M. Cholasinski, *Geometry of an adiabatic passage at a level crossing*, *Phys. Rev. A* **71**, 063409 (2005).
 - [60] J. E. Avron, M. Fraas, G. M. Graf, and P. Grech, *Adiabatic theorems for generators of contracting evolutions*, *Commun. Math. Phys.* **314**, 163 (2012).
 - [61] E. Farhi, J. Goldstone, S. Gutmann, and M. Sipser, *Quantum computation by adiabatic evolution*, *arXiv:0001106 [quant-ph]* (2000).
 - [62] J. Roland and N. J. Cerf, *Quantum search by local adiabatic evolution*, *Phys. Rev. A* **65**, 042308 (2002).
 - [63] S. Jansen, M. B. Ruskai, and R. Seiler, *Bounds for the adiabatic approximation with applications to quantum computation*, *J. Math. Phys.* **48**, 102111 (2007).
 - [64] N. Wiebe and N. S. Babcock, *Improved error-scaling for adiabatic quantum evolutions*, *New J. Phys.* **14**, 013024 (2012).
 - [65] O. Higgott, D. Wang, and S. Brierley, *Variational Quantum Computation of Excited States*, *Quantum* **3**, 156 (2019).
 - [66] K. M. Nakanishi, K. Mitarai, and K. Fujii, *Subspace-search variational quantum eigensolver for excited states*, *Phys. Rev. Res.* **1**, 033062 (2019).
 - [67] P. Weinberg and M. Bukov, *QuSpin: A Python package for dynamics and exact diagonalisation of quantum many body systems part I: Spin chains*, *SciPost Phys.* **2**, 003 (2017).
 - [68] P. Weinberg and M. Bukov, *QuSpin: A Python package for dynamics and exact diagonalisation of quantum many body systems. Part II: Bosons, fermions and higher spins*, *SciPost Phys.* **7**, 020 (2019).
 - [69] P. Weinberg, M. Schmitt, and M. Bukov, *QuSpin documentation*, <http://quspin.github.io/QuSpin/>.
 - [70] J. R. Johansson, P. D. Nation, and F. Nori, *QuTiP: An open-source Python framework for the dynamics of open quantum systems*, *Comp. Phys. Comm.* **183**, 1760 (2012).
 - [71] J. R. Johansson, P. D. Nation, and F. Nori, *QuTiP 2: A Python framework for the dynamics of open quantum systems*, *Comp. Phys. Comm.* **184**, 1234 (2013).
 - [72] J. R. Johansson, *Lectures on QuTiP: Lecture 8 - Adiabatic sweep*, <https://github.com/jrjohansson/qutip-lectures/blob/master/Lecture-8-Adiabatic-quantum-computing.ipynb>.
 - [73] A. Javadi-Abhari, M. Treinish, K. Krsulich et al., *Quantum computing with Qiskit*, *arXiv:2405.08810* (2024).

- [74] N. Hatano and M. Suzuki, *Finding exponential product formulas of higher orders*, [Quantum annealing and other optimization methods](#) (Springer Berlin Heidelberg, 2005).
- [75] D. W. Berry, G. Ahokas, R. Cleve, and B. C. Sanders, *Efficient quantum algorithms for simulating sparse Hamiltonians*, [Commun. Math. Phys.](#) **270**, 359 (2007).
- [76] Y. Li and S. C. Benjamin, *Efficient variational quantum simulator incorporating active error minimization*, [Phys. Rev. X](#) **7**, 021050 (2017).
- [77] K. Temme, S. Bravyi, and J. M. Gambetta, *Error mitigation for short-depth quantum circuits*, [Phys. Rev. Lett.](#) **119**, 180509 (2017).
- [78] T. Giurgica-Tiron, Y. Hindy, R. LaRose et al., *Digital zero noise extrapolation for quantum error mitigation*, [2020 IEEE International Conference on Quantum Computing and Engineering \(QCE\)](#), 306 (2020).
- [79] R. Majumdar, P. Rivero, F. Metz et al., *Best practices for quantum error mitigation with digital zero-noise extrapolation*, [arXiv:2307.05203](#) (2023).
- [80] V. Sazonov and M. Tamaazousti, *Quantum error mitigation for parametric circuits*, [Phys. Rev. A](#) **105**, 042408 (2022).